Materials Science & Engineering A 559 (2013) 655–664

Contents lists available at SciVerse ScienceDirect

Materials Science & Engineering A

journal homepage: www.elsevier.com/locate/msea

# Texture and temperature dependence on the mechanical characteristics of copper electrodeposits

Jenn-Ming Song [a,*], Ding-Siang Wang [b], Chung-Hsien Yeh [b], Wei-Chih Lu [b], Yung-Sheng Tsou [b], Shi-Ching Lin [c]

[a] Department of Materials Science and Engineering, National Chung Hsin University, Taichung 402, Taiwan
[b] Department of Materials Science and Engineering, National Dong Hwa University, Hailien 974, Taiwan
[c] Electro Mtls Div Copper Foil Tech., Nan Ya Plastics Corporation, Jiayih 616, Taiwan

ARTICLE INFO

*Article history:*
Received 9 May 2012
Received in revised form
3 September 2012
Accepted 4 September 2012
Available online 12 September 2012

*Keywords:*
Cu electrodeposit
Preferred orientation
Nanoindentation
Tensile property

ABSTRACT

The relationships between grain morphology, preferred orientation, and mechanical performance of commercial grade electrodeposited Cu foils (VLP, MP and HTE) were clarified in this study. Electrodeposited Cu foils showing (220) and (111) growth textures had fine grains of which the distribution was fan-shaped or well-aligned along the through-thickness direction respectively. On the other hand, the (200)-oriented Cu foils consisted of randomly grown coarse grains. Electron backscatter diffraction (EBSD) analysis of the cross-sectioned foils revealed that all the samples exhibited diffuse in-plane texture (on the plane of the foils). The growth texture of the Cu grains dominated Young's modulus of the foils measured by nanoindentation along the through-thickness direction of the Cu foils, in decreasing order was (111), (220) and then (200) oriented foils. With respect to tensile properties, the effect of grain size was more pronounced for tensile strength. The (220)-oriented Cu foils possessed a superior combination of tensile strength and ductility. However, the (200)-oriented foils exhibited a poorer deformation resistance but a lower strength loss at elevated temperatures. Serration in the tensile stress–strain curves could be observed at 150 °C and became intense at 250 °C. In addition to dynamic strain aging, low temperature dynamic recrystallization also accounted for this instability in flow stress.

© 2012 Elsevier B.V. All rights reserved.

## 1. Introduction

Due to excellent electrical and thermal conductivities, Cu foils have been widely applied as the conductive layers of printed circuit boards [1]. Due to the tremendous developments in IC and electronic packaging technologies, the miniaturization of microelectronic interconnections has become an important trend. To fulfill the demand for conductor patterns with fine pitch and high density, the performance of Cu foils plays an important role [2].

Nowadays most of the Cu foils for PCB applications are manufactured by the electro-deposition method. As sketched in Fig. 1, Cu is electrodeposited on a titanium drum acting as the cathode from an acid copper sulfate, for example, $CuSO_4$. A dimensional stable anode (DSA, $Ta_2O_5$ and $IrO_2$) is used as the insoluble anode. The microstructural characterization of the electrodeposits such as texture, grain and surface morphologies are strongly influenced by electrolysis conditions (bath composition, pH, overpotential, current density, additives, etc.) [3–7]. Take the texture for example, it has been suggested that electrodeposition can generate a variety of fiber textures. As for Cu deposits, the preferred orientation shifts from ⟨110⟩, ⟨100⟩ to ⟨111⟩ with an increasing overvoltage [8].

How those structural features affect the physical and mechanical performance has attracted considerable attention [9–11], but the relationship between preferred orientation and mechanical performance of the ED Cu foils still remains elusive. To clarify the dependence of growth texture on the mechanical performance, including hardness, Young's modulus and tensile behavior of electrodeposited Cu foils (ED Cu foils), three types of commercial grade Cu foils were selected for this investigation. As illustrated in Fig. 2, with increasing surface roughness as well as peel strength with polymeric substrates, they were VLP (very low profile), MP (middle profile) and HTE (high temperature elongation). Considering that Cu foils are often subjected to mechanical and thermal loading [12–15], the tensile tests were also performed at elevated temperatures, 150 °C and 250 °C, to simulate the operation conditions of electronic devices and multiple reflows during assembly.

## 2. Experimental procedures

Rather than the laboratory-prepared foil samples, commercial grade Cu foils (VLP, MP and HTE) with average thickness of 18 μm

* Corresponding author. Tel.: +886 4 22852482; fax: +886 4 22857017.
*E-mail address:* samsong@nchu.edu.tw (J.-M. Song).

0921-5093/$ - see front matter © 2012 Elsevier B.V. All rights reserved.
http://dx.doi.org/10.1016/j.msea.2012.09.006



SOLUS-1009

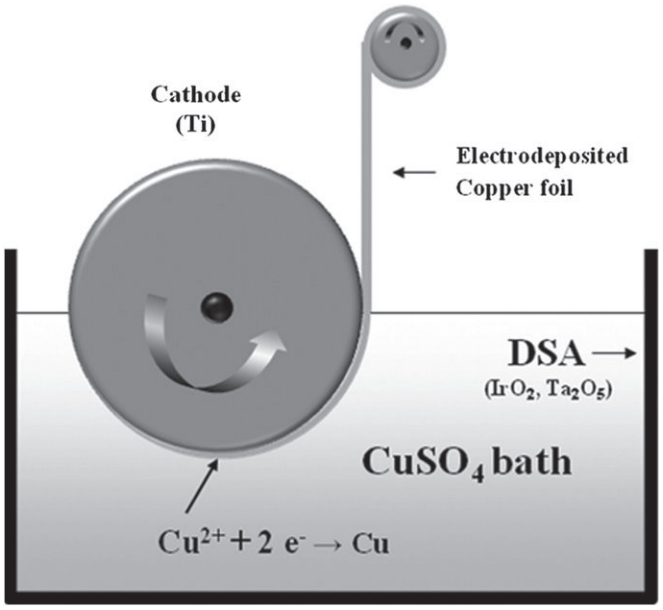



**Fig. 1.** Schematic diagram of the electroplating process for Cu foils (DSA: dimensional stable anode).

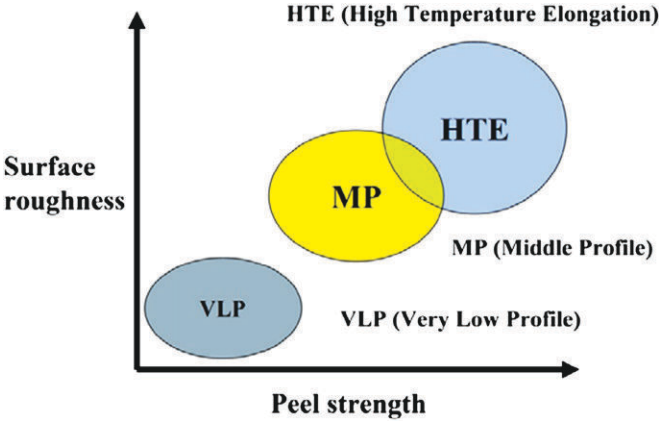



**Fig. 2.** Properties of commercial Cu foils for PCB applications.

were obtained from industry and adopted as testing materials. The deposition parameters and the additives employed were proprietary. With various fabrication conditions, there were four kinds of VLP samples, namely VLP-A, VLP-B, VLP-C and VLP-D. The surface attached to the titanium drum was designated as the shiny side, while the other exposed in the electrobath was the matte side. For the as-received Cu foils, the thermal barrier and passivation layers, mainly comprising Cr and Zn tens of nanometers in thickness, were applied to prevent oxidation and reaction with polymeric substrates [16]. Parts of the VLP-D foils were subjected to a pre-annealing treatment which was carried out at 650 °C for 1 h in vacuum to obtain the full annealed structure.

X-ray diffraction (XRD) was applied to characterize the grain orientation. The growth texture of the Cu foils was evaluated by the texture coefficient (TC), which can be calculated using the equation below.

$$TC_{hkl} = \frac{I_{hkl}/I^o_{hkl}}{(1/n)\sum(I_{hkl}/I^o_{hkl})}$$

where $I_{hkl}$ is the measured integrated X-ray intensity of the ($hkl$) plane and $I^o_{hkl}$ is the integrated X-ray intensity of the isotropic powder specimens, and $n$ is the number of diffraction peaks. When the TCs of all reflection planes are the same, the distribution of crystal orientation is random. When the TC of any ($hkl$) plane is larger than the mean value of TCs, a preferred orientation or a texture exists in which the [$hkl$] directions of grains are parallel to the through-thickness direction of the foils, regarded as the out-of-plane texture of the Cu foils. The larger the value of TC, the greater the degree of preferred orientation.

A scanning electron microscope (SEM) equipped with electron backscatter diffraction (EBSD) was used to observe the cross-sectional microstructures and analyze the in-plane texture (perpendicular to the through-thickness direction). Cross-sectioning was performed by a cross-section polisher with an argon beam. The principle and practice of EBSD are described in detail elsewhere [17]. The EBSD data was noise reduced using the 'Tango' module of HKL Technology's CHANNEL5 software.

The thermal behavior of the foils was analyzed using differential scanning calorimetry (DSC, Setaram Labsy DSC) in nitrogen. The specimens with weight of 100 mg were heated to 700 °C with a constant heating rate of 5 °C/min. X-ray photoelectron spectroscopy (XPS) with Mg sources (Thermo Scientific K-Alpha) was employed to investigate the chemical valence states of the elements on the sample surface.

Hardness and Young's modulus were evaluated by nanoindentation testing on the shiny side of the foils along the through-thickness direction using a MTS Nano indenter XP with a Berkovich tip (tip radius 20 nm). A continuous stiffness measurement (CSM) technique was used during indentation. A purely isotropic silica standard was used to calibrate the system. The loading rate of the indent was 5 nm/s, and the loading continued until a total indenter displacement was reached (500 nm in this study). The load–displacement data obtained were analyzed using the method of Oliver and Pharr [18] to determine the hardness and the Young's modulus as a function of the displacement of the indenter. Each datum was the average of at less five tests.

Tensile tests of the free standing Cu foils were performed using rectangular specimens (gauge length section: 20 mm × 5 mm × 18 μm). The initial tensile strain rate was kept at $1.67 \times 10^{-3}\ s^{-1}$. Testing temperatures were set as room temperature, 150 °C (the operation temperature of devices) and 250 °C (the reflow temperature during assembly). All the tensile tests were carried out after a 5-min equilibrium at the set temperature.

## 3. Results and discussion

### 3.1. Microstructural characteristics and thermal properties

The XRD patterns shown in Fig. 3 indicate that three low-indexed diffraction peaks, (111), (200) and (220) could be identified for the ED Cu foils. The texture coefficients of those crystallographic planes were calculated and tabulated in Table 1. When those data were combined with microstructural observations (Figs. 4–6), the Cu foils could be categorized based on the grain morphology and preferred orientation. As illustrated in Fig. 4, the fan-like distributed columnar grains of the HTE, MP and VLP-A samples were with (220) preferred orientation. The (200) oriented samples, VLP-B and VLP-C, showed a less-well-developed columnar structure and were with relatively diffused growth direction (Fig. 5). Notably, sample VLP-D exhibited a strong (111) texture and possessed extremely fine grains grown along the through-thickness direction (Fig. 6(a)). Subjected to isothermal heating at 650 °C for 1 h, Fig. 6(b) illustrates the fully annealed structure of VLP-D foils, with the coarsened grains stretching across the foil.

With regards crystallographic and microstructural information, Fig. 7 illustrates the crystal orientation maps and corresponding inverse pole figures of the cross-sections of selected ED Cu foil samples, (220)-oriented HTE, (200)-oriented VLP-C and

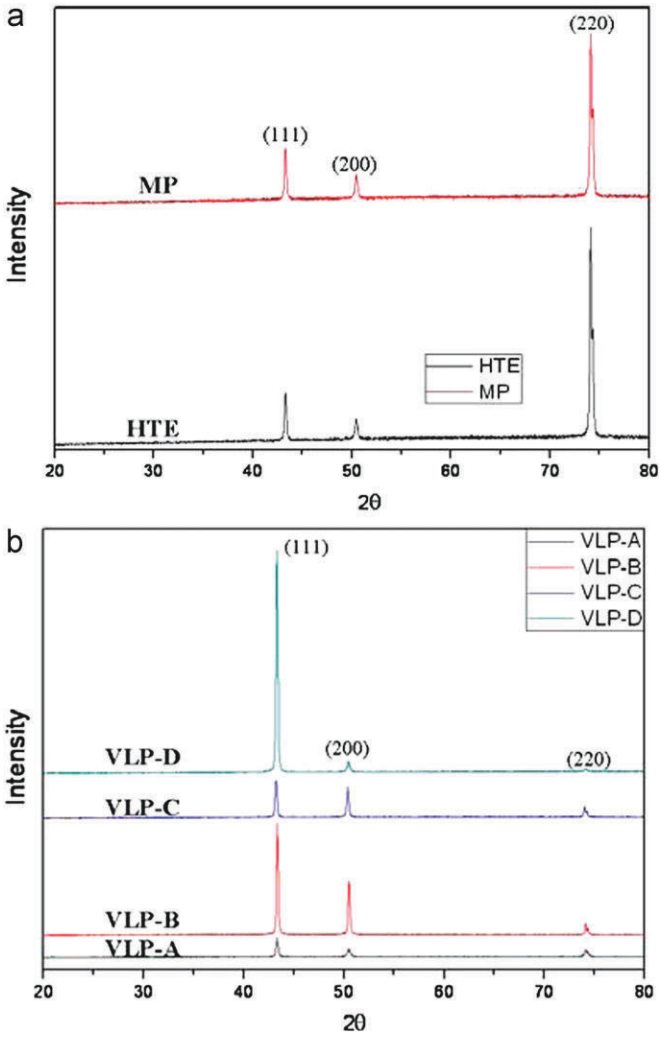



**Fig. 3.** X-ray diffraction patterns of the Cu foils: (a) HTE and MP, (b) VLP series.

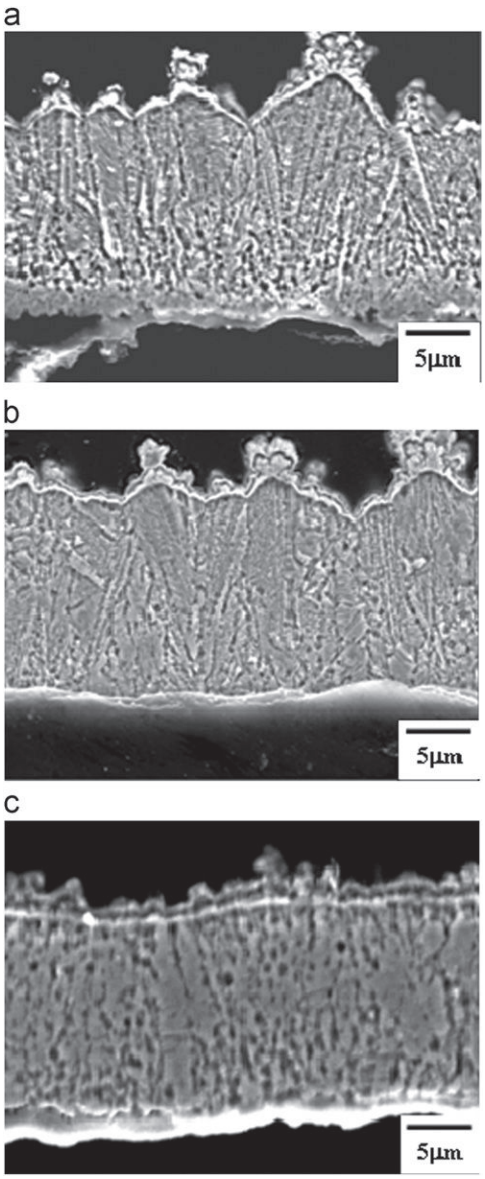



**Fig. 4.** Cross-sectional microstructure of (220) oriented foils (a) HTE, (b) MP and (c) VLP-A.

**Table 1**
Calculated textural coefficients of ED foils.

| | HTE | MP | VLP-A | VLP-B | VLP-C | VLP-D |
|---|---|---|---|---|---|---|
| **(111)** | 0.173 | 0.221 | 0.74 | 1.118 | 0.684 | **2.398** |
| **(200)** | 0.199 | 0.265 | 0.782 | **1.232** | **1.268** | 0.312 |
| **(220)** | **2.628** | **2.515** | **1.487** | 0.65 | 1.084 | 0.291 |

(111)-oriented VLP-D. According to the color of the grain images, the Cu grains exhibited various morphologies. Similar to what was revealed in the above SEM images, (220)-oriented HTE did possess fan-like distributed fine-elongated columnar grains, except for some small equi-axed grains at the bottom of the foils (Fig. 7(a)). In addition, large grains were observed in the (200)-oriented VLP-C (Fig. 7(b)), while fine equi-axed grains could be recognized in the (111)-oriented foils (Fig. 7(c)). Combined with the SEM image shown Fig. 6(a), it can be inferred that those fine grains had a directional arrangement from a macro viewpoint. EBSD statistic results indicate that the average grain area and average grain size were 0.24 $\mu m^2$ and 0.41 μm for HTE, 1.2 $\mu m^2$ and 0.55 μm for VLP-C, 0.28 $\mu m^2$ and 0.44 μm for VLP-D. It should be noted that the inverse pole figures taken from the cross-sections (Fig. 7(d)–(f)) indicate that all these Cu foils possessed diffuse in-plane textures (on the plane of the Cu films) even though they exhibited distinct growth textures along the through-thickness direction.

Table 2 lists the chemical composition of the sub-surface region on the shiny side of the samples, which was about 100 nm deep from the surface after $Ar^+$ ion bombardment for removal of the heat-resistant coating. O, N, and Cl can be ascribed to the residue of chemical additives, while the existence of Zn and Cr may have resulted from the inward diffusion of the thermal barrier coating. Zn is more likely to dissolve into Cu rather than to form compounds due to its remarkable solid solubility up to 38.3 at%, which is much higher than that of Cr (about 0.89 wt%) [19]. This can be verified by the binding energy values of the XPS peaks given in Fig. 8, indicating that Zn remained in its elemental state ($Zn2p_{1/2}$: 1045.1, $Zn2p_{3/2}$: 1021.61 [20]).

Fig. 9 shows DSC curves of the foils upon heating to 600 °C. Wedge-shaped exothermic peaks were detected for all the foils, which can be regarded as the release of stored energy. By computing the peak area of the DSC curves, the stored energies of the foils were estimated ranging from 7.6 J/mole to 16.1 J/mole; it seems to have no direct relation with the texture. Interestingly,

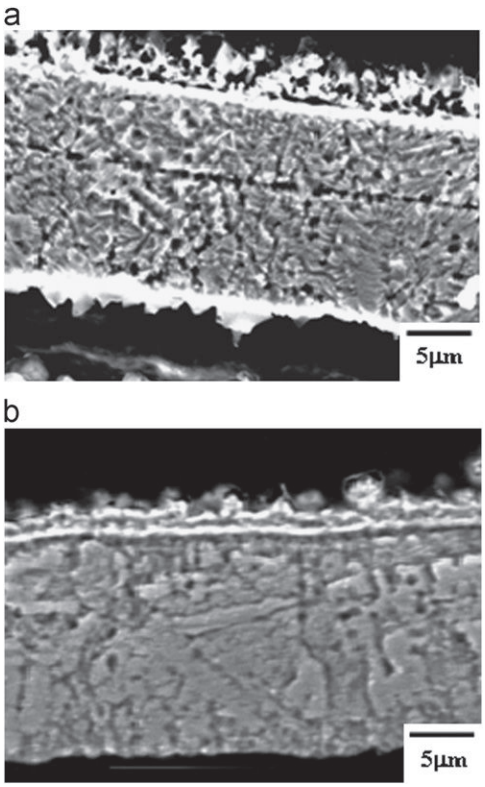



**Fig. 5.** Cross-sectional microstructure of (200) oriented foils (a) VLP-B and (b) VLP-C.

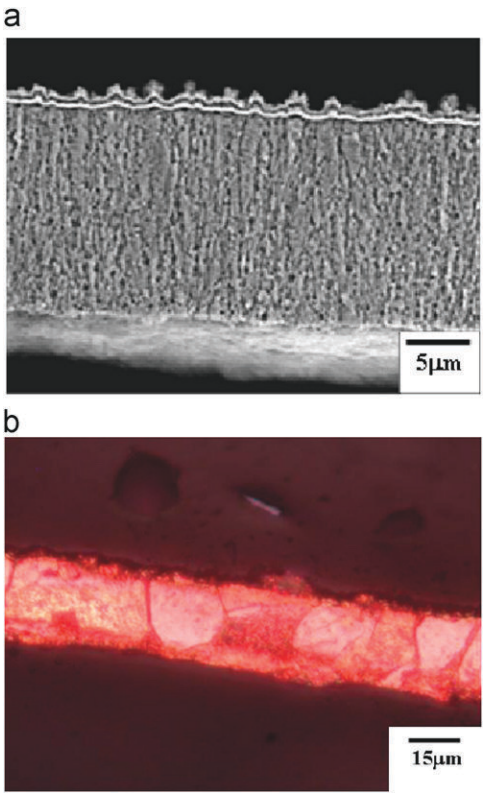



**Fig. 6.** VLP-D foils: (a) as-deposited samples with (111) preferred orientation, and (b) annealed samples.

the exothermic reaction of VLP-B started at a temperature slightly lower than 300 °C, while for the others the onset temperature was located between 300 °C and 350 °C. The stored energy, mostly the contribution of dislocations, is released when the temperature becomes sufficient to allow the relaxation processes (recovery and recrystallization) to occur [7,21]. It indicates that the recovery and recrystallization of the ED foils took place at temperatures much lower than bulk copper.

### 3.2. Mechanical properties

The response of nanoindentation tests on the shiny side of the foils are listed in Table 3 and Fig. 10. Compared to hardness, the data of Young's modulus show a stronger orientational dependence. The foils with strong (111) texture and medium grain size exhibit the greatest stiffness, while the foils with diffuse (200) texture show a relatively lower modulus. This leads us to believe that instead of the grain size, the difference in the modulus of the Cu foils can be ascribed to the effect of growth texture. That is, for most cubic materials $E_{\langle 111\rangle}$ (i.e., the modulus measured with the stress axis along the $\langle 111\rangle$ direction) is larger than $E\langle 100\rangle$, and the modulus along an arbitrary [*hkl*] direction is between these two extremes [22]. This tendency also holds for Cu. Young's modulus of Cu in an arbitrary direction [*hkl*] could be calculated in terms of stiffnesses or compliances and the orientation of the [*hkl*] to the three $\langle 100\rangle$ directions using the following equation [22]:

$$\frac{1}{E_{[hk]}} = S_{11} - 2\left(S_{11} - S_{12} - \frac{1}{2}S_{44}\right)(\alpha^2\beta^2 + \alpha^2\gamma^2 + \beta^2\gamma^2)$$

where $S_{11}$, $S_{12}$ and $S_{44}$ are independent compliances. $\alpha$, $\beta$, and $\gamma$ are the direction cosine of the [*hkl*] direction and the [100], [010] and [001] directions, respectively. The moduli thus obtained are 66.7 GPa for $E_{[100]}$, 130.2 GPa for $E_{[110]}$, and 190.84 GPa for $E_{[111]}$, of which the order is consistent with the measured data in this study. The calculated values for modulus are not exactly identical to those obtained from nanoindentation. This is because the calculation of theoretical modulus is based on the assumption that all the FCC Cu crystals are arranged along a specific crystallographic direction. However, in the case of electrodeposits, the Cu foils comprised the grains with different textures. For each foil, one of the textures was dominated, but there was still a portion of grains with other growth directions.

Fig. 11 illustrates the stress–strain curves of the samples tested at various temperatures. Remarkably, the tensile curves at elevated temperature show a serrated flow feature and the degree of jerking became more intense with a higher temperature. The measured tensile strengths (yield strength (YS), ultimate tensile strength (UTS)) and elongation are given in Figs. 12 and 13 respectively. Tensile strength decreased as the testing temperature rose due to matrix softening. At room temperature and 150 °C, the (200)-oriented samples with coarse grains possessed a relatively lower deformation resistance. On the other hand, (220)-oriented foils showed comparable or even higher tensile strength than (111)-oriented samples. This implies that unlike the nanoindentation data which were obtained along the through-thickness direction and dependent upon out-of-plane texture, tensile strength can be correlated to the grain size more closely since the in-plane texture was diffuse and thus made less of a contribution. However, the UTS and YS of all the samples tended to be identical at 250 °C. This may somehow demonstrate that recrystallization or grain growth occurred, and consequently there was no longer any contribution from grain size and texture. With respect to the elongation (Fig. 13), all in all, (220)-oriented foils had better ductility within the testing temperature range. This may somehow be ascribed to the textural strengthening of

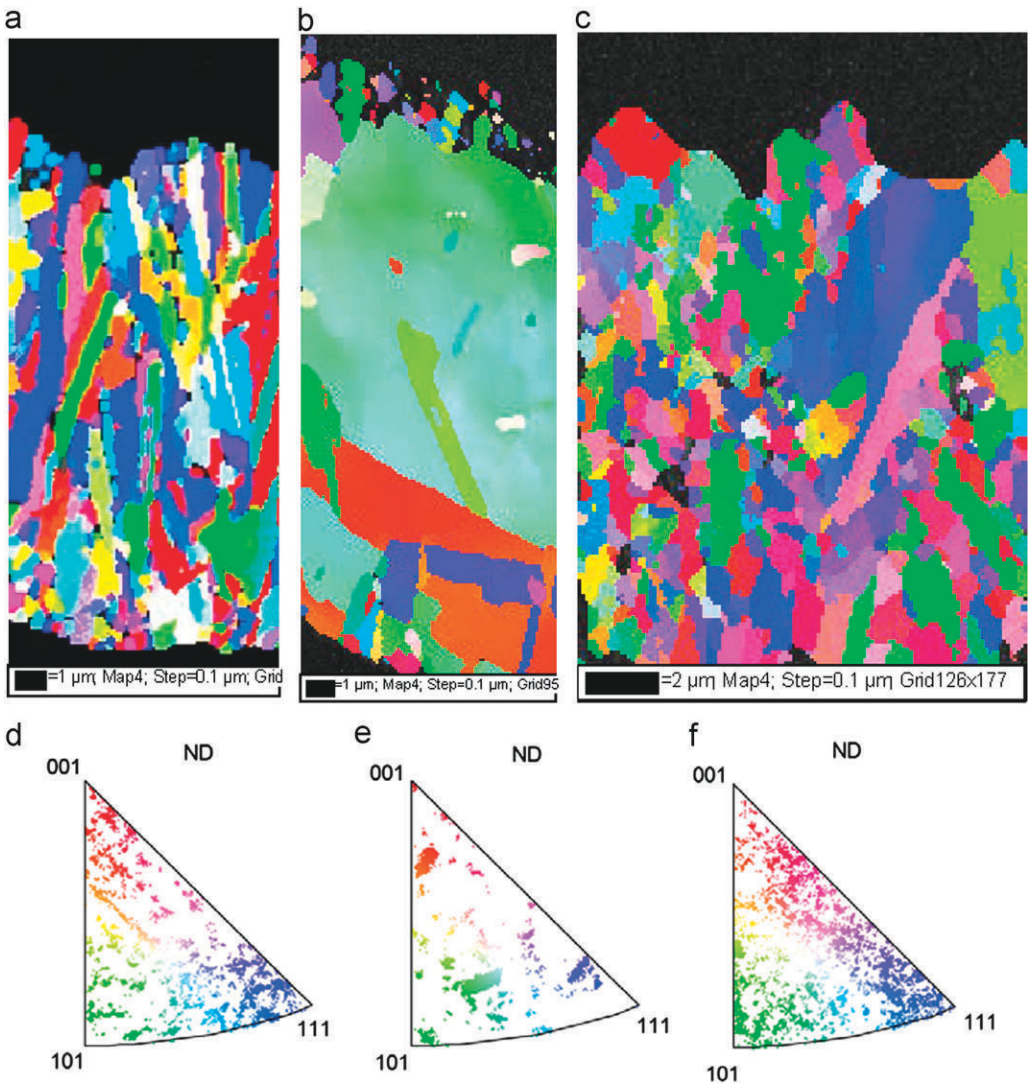



**Fig. 7.** EBSD images and inverse pole figures of the selected Cu foils: (a and d) HTE (220), (b and e) VLP-C (200) and (c and f) VLP-D (111) (ND: normal direction to the cross-sectioned plane).

**Table 2**
Chemical composition of the subsurface regions analyzed by XPS (signal obtained from 100 nm depth underneath the surface).

| sample (at%) | Zn | Cr | O | N | Cl | Cu |
|---|---|---|---|---|---|---|
| **HTE (220)** | 1.28 | 1.29 | 3.23 | 1.23 | 0.74 | Bal. |
| **MP (220)** | 0.95 | 1.32 | 2.50 | 1.54 | 0.60 | Bal. |
| **VLP-A (220)** | 0.85 | 1.10 | 2.30 | 0.95 | 1.50 | Bal. |
| **VLP-B (200)** | 1.01 | 1.73 | 2.65 | 1.25 | 0.67 | Bal. |
| **VLP-C (200)** | 1.03 | 1.20 | 2.67 | 1.03 | 0.59 | Bal. |
| **VLP-D (111)** | 0.73 | 1.12 | 3.17 | 1.64 | 0.70 | Bal. |

(220)-oriented foils. Subjected to true plastic strain of 2% at 150 °C, work hardening rate ($n$ value) was 0.69 for HTE ((220) foils), 0.44 for VLP-C ((200) foils) and 0.57 ((111) foils) for VLP-D. It is known that a higher $n$ value contributes to better ductility [23]. Even though texture is not the key factor affecting work hardening rate like grain size [24,25], we still can suggest that foils with stronger preferred orientation possess greater ability for work hardening and thus better elongation. However, both the textural and grain size effects decayed at elevated temperatures. All in all, it can be deduced that (220)-oriented foils had a better combination of tensile strength and ductility.

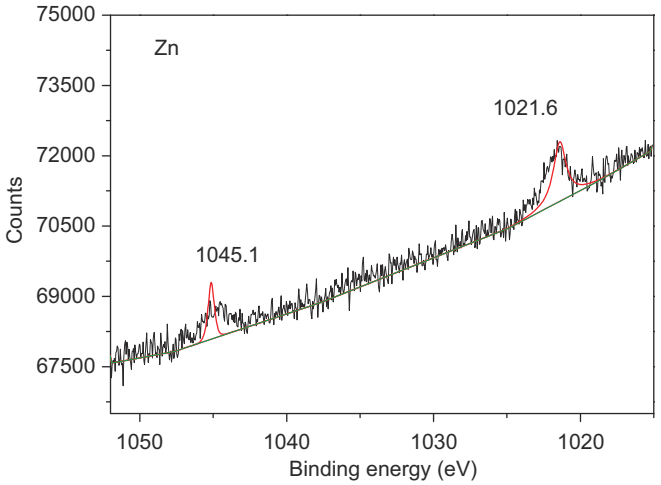



**Fig. 8.** Zn2p signal on the XPS spectrum for the VLP-B samples.

The variation of tensile strength and elongation against test temperature are illustrated in Figs. 14 (a), (c), (e). By unification of the data obtained at room temperature, Figs. 14 (b), (d), (f) give

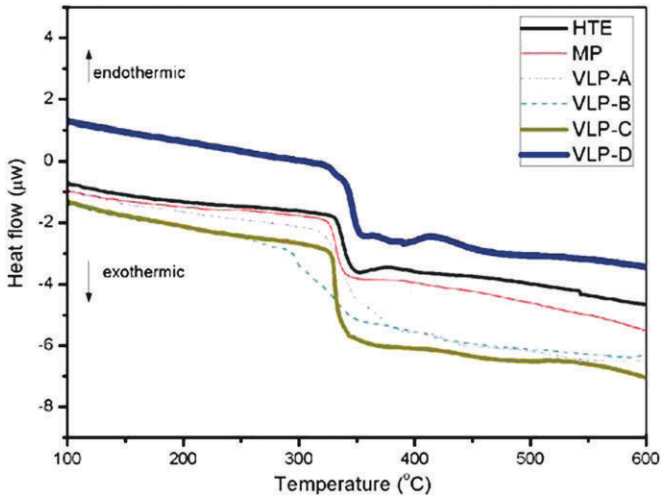



**Fig. 9.** DSC curves upon heating.

**Table 3**
Hardness and modulus obtained by nanoindentation.

| | Hardness (GPa) | Modulus (GPa) |
|---|---|---|
| **HTE (220)** | 1.727 ± 0.049 | 100.579 ± 3.092 |
| **MP (220)** | 1.726 ± 0.037 | 104.778 ± 1.985 |
| **VLP-A (220)** | 2.20 ± 0.057 | 101.275 ± 2.139 |
| **VLP-B (200)** | 1.472 ± 0.066 | 97.783 ± 4.951 |
| **VLP-C (200)** | 1.842 ± 0.092 | 88.185 ± 4.806 |
| **VLP-D (111)** | 1.962 ± 0.071 | 112.091 ± 4.638 |

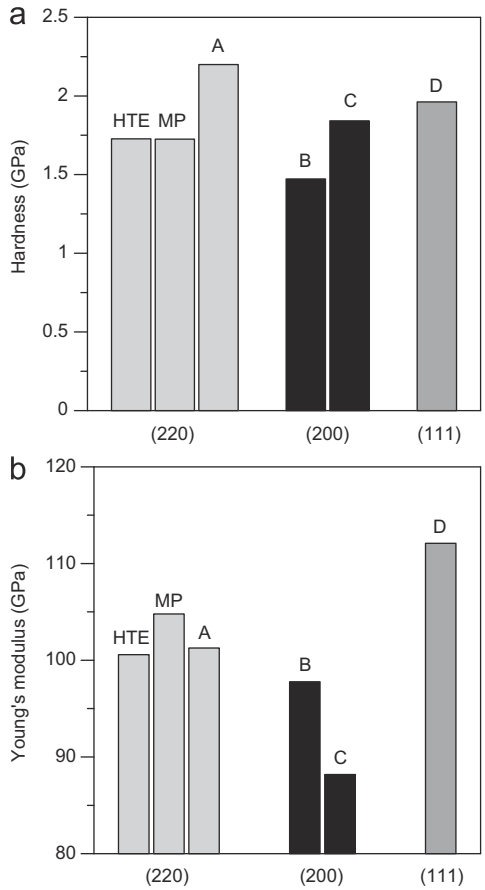



**Fig. 10.** Nanoindentation responses on the shiny side of the Cu foils: (a) hardness, and (b) Young's modulus.

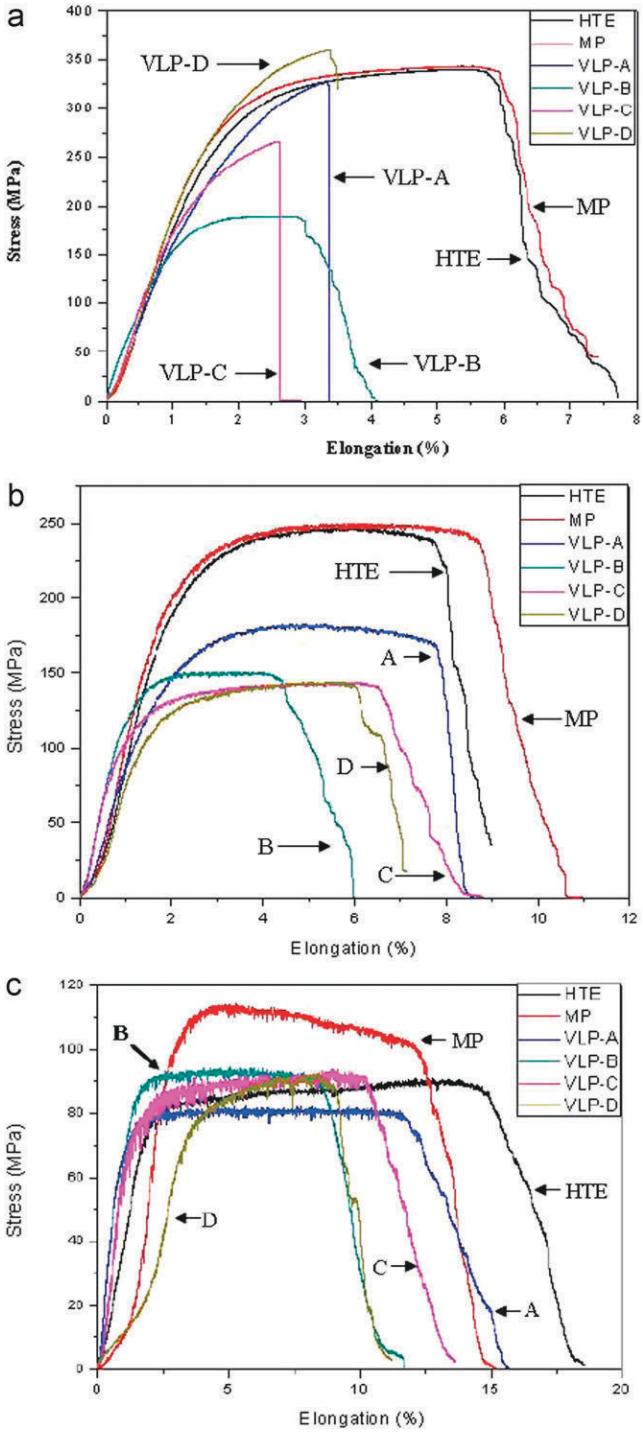



**Fig. 11.** Tensile stress–strain curves at different testing temperatures: (a) room temperature, (b) 150 °C and (c) 250 °C.

the strength loss and the elongation gain respectively as a function of tensile temperature. It can be found that MP and the (200) oriented samples, VLP-B and VLP-C, suffered a smaller loss in tensile strength. As aforementioned, the effects of texture and grain size decayed at elevated temperatures. That is why the (200)-oriented foils with coarse grain and small texture coefficient possessed lower strength loss. Furthermore, all the samples exhibited enhanced ductility at elevated temperatures. The VLP-C had the greatest increase in elongation, up to 400% at 250 °C, while the smallest boost of about 100% could be observed for MP.

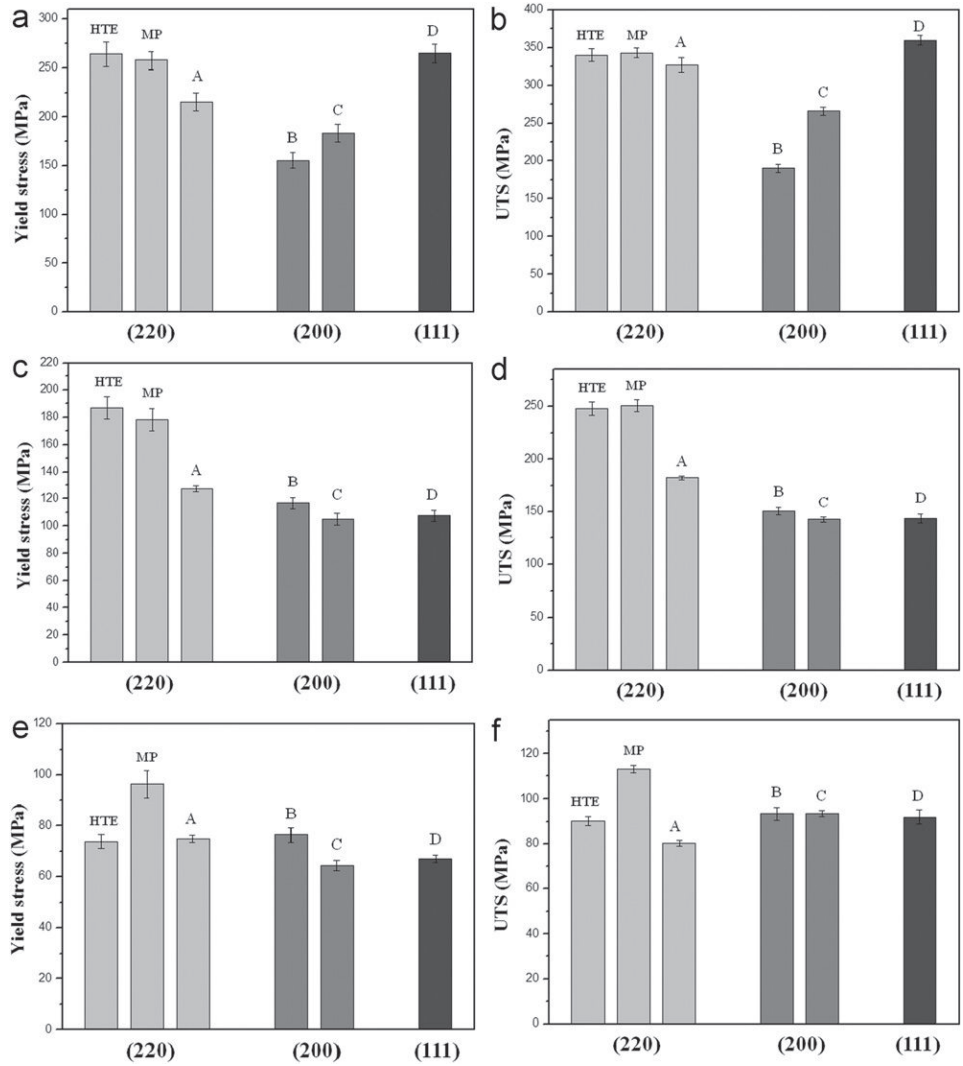



**Fig. 12.** Yield stress and ultimate tensile strength of the foils at different testing temperatures: (a and b) room temperature, (c and d) 150 °C and (e and f) 250 °C.

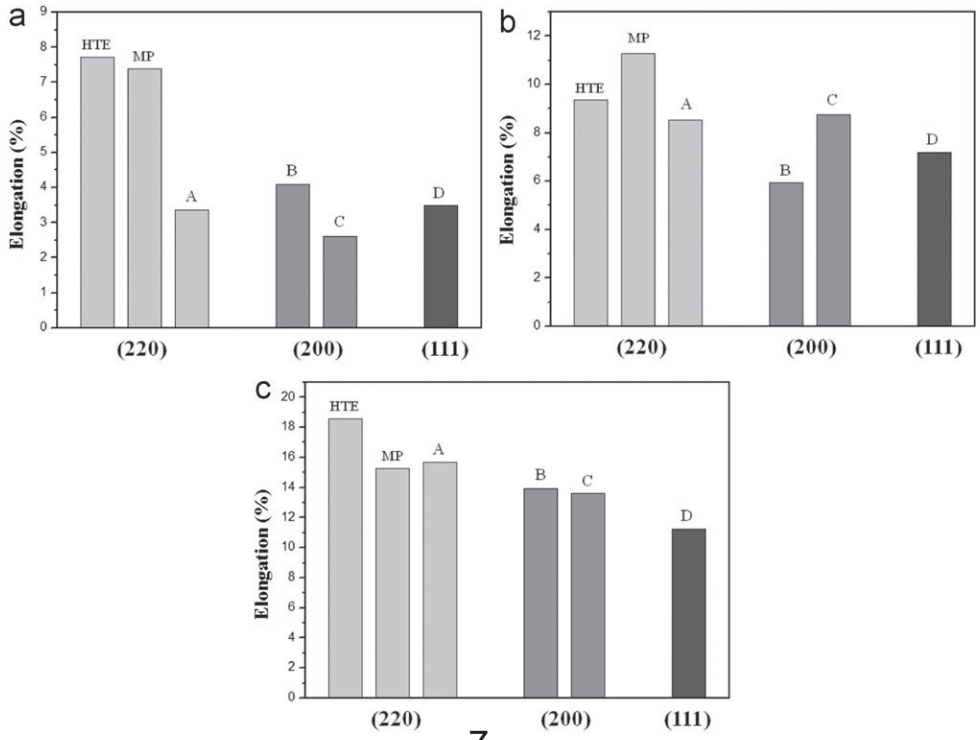



**Fig. 13.** Total elongation of the foils at different testing temperatures: (a) room temperature, (b) 150 °C and (c) 250 °C.

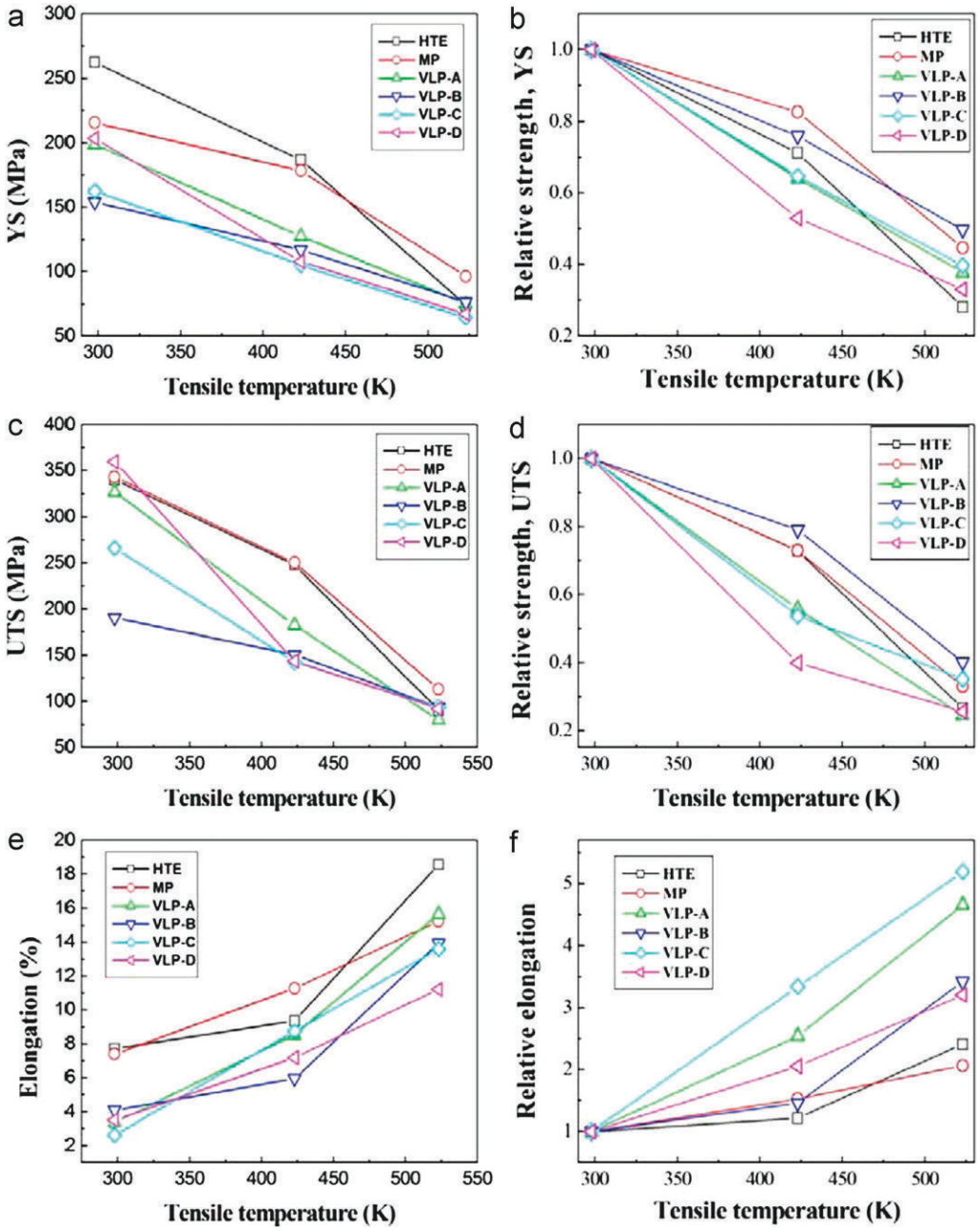



**Fig. 14.** Variation in tensile properties and their relative values with respect to test temperature: (a and b) yield strength, (c and d) ultimate tensile strength and (e and f) elongation gain.

The 180 °C embrittlement of the copper electrodeposits noted in previous reports, which was mainly due to incorporation of hydrogen during deposit growth [15], did not happen here.

### 3.3. Formation of serrated flow

As mentioned above, serrated flows appeared in the tensile curves obtained at 150 °C and 250 °C. The instability in flow stress reflects the inhomogeneity of plastic deformation which may be raised by deformation twinning, dynamic recrystallization (DRX), dynamic strain aging (DSA) and so forth [26,27]. To clarify the mechanism, Fig. 15 compares tensile curves of as-deposited and pre-annealed VLP-D foils at elevated temperatures; the pre-annealed samples show an inferior deformation resistance. Worthy of note is that the serration of flow stress could still be observed but with a reduced intensity for the pre-annealed foils, as indicated in the magnified tensile curves (Fig. 15(b)).

Previous studies suggested that recrystallization of electroplated Cu may result at temperatures lower than the theoretical value (1/2 Tm) mainly due to the residual stress and also the peculiar defect-saturated structure [13,14]. The activation energy is considerably less, by a factor of two or three, than that for recrystallization of the bulk wrought copper. This could be demonstrated by our observation on exothermic behavior at around 300 °C upon heating. It can be inferred that the starting temperature for dynamic recrystallization (DRX) was further depressed, and thus low temperature DRX may account for the serration of tensile flow to some extent.

As mentioned above, the pre-annealed foils with strain-free large Cu grains, jerky flows could still occur (Fig. 15(a) and (b)), but the amplitude of serration was significantly diminished.

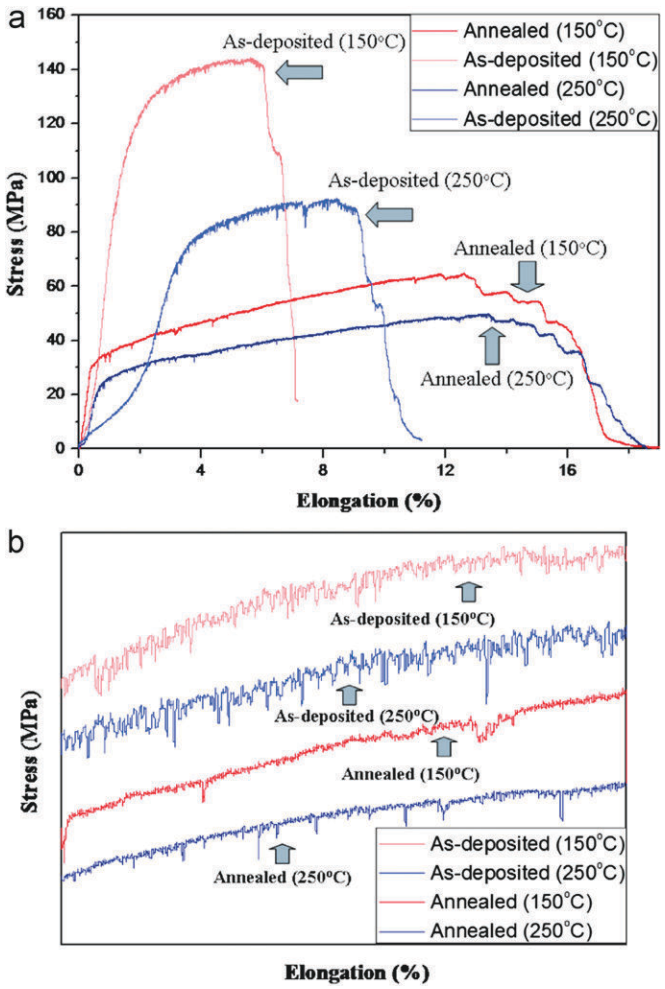



**Fig. 15.** (a) Tensile stress and strain curves of as-deposited and annealed VLP-D samples, and (b) serrate flows on enlarged curves.

This implies that in addition to DRX, there must be other factors resulting in instability of the flow stress. Considering the Portevin–Le Chatelier effect, which is also known as dynamic strain aging (DSA), the PLC effect mainly occurs in two types of alloys, BCC metals containing interstitial solutes and FCC metals containing substitutional solutes [26]. Corresponding to the latter case, the solved Zn atoms in Cu from the surface coating (Fig. 8) likely reacted with the dislocations, contributed to a drag force affecting the dislocation glide and thus gave rise to dynamic strain aging and thus unstable flow stress.

A previous report concerning the DSA in alpha-brass (Cu-32 wt%Zn) verified that serrated flow could be detected in the temperature range between −25 °C and 275 °C with a strain rate of $4.76 \times 10^{-4}\ s^{-1}$, slightly slower than what we used in this study [28]. It also pointed out that four types of serrations on the stress–strain curve could be identified, two of which appeared at high temperatures. One is with quick oscillation in flow stress at the average level, and the other which emerges at the highest temperature (275 °C) appears as a sudden drop in flow stress to below the average. The sharp drop was ascribed to the formation of new dislocations having no drag from solute clouds. However, new dislocations will be aged quickly and thus the stress rises quickly to the average level of the curve. Those characteristics are consistent with what we observed in the flow charts of annealed Cu foils at 150 °C and 250 °C. Therefore, it can be concluded that the serrated flow of ED Cu foils resulted from the combined effect of DRX and DSA. These two phenomena contributed to opposite influences on mechanical properties. DRX gives rise to softening [29], while DSA causes strengthening [30].

## 4. Conclusions

In this study, the microstructural characteristics and mechanical properties (nanoindentation and tensile behavior) of the electro-deposited Cu foils with various preferred orientations were investigated. EBSD observation results indicate that the foils with (220) texture exhibited a fan-like arrangement of fine columnar grains. The (200) oriented grains were coarse and randomly grown. The fine grains in the (111) oriented foils were equi-axed but grew along the through-thickness direction. There existed a close relationship between the preferred orientation and indentation modulus of the electro-deposited foils with the approaching direction normal to foil surface. Young's modulus in decreasing order was (111), (220) and then (200) oriented foils. With respect to the tensile properties, grain size had a pronounced effect on tensile strength because all the foils possessed diffusion in-plane texture. In general, (220)-oriented foils had the superior combination of tensile strength and ductility. Those with the (200) texture possessed a lower strength loss at elevated temperatures. Worthy of notice is, when tested at 150 °C and above, serrated flows on the tensile curves could be observed, which may have resulted from the combined effect of dynamic recrystallization (DRX) and dynamic strain aging (DSA).

## Acknowledgments

This work has been supported by the National Science Council of R.O.C. (Contract: NSC 99-2221-E-005-119-MY2), for which the authors are grateful.

## References

[1] B. Weiss, V. Gröger, G. Khatibi, A. Kotas, P. Zimprich, R. Sticker, B. Zagar, Sensors Actuators A: Phys. 99 (2002) 172–182.
[2] H.J. Lee, H.N. Han, D.N. Lee, J. Electron. Mater. 34 (2005) 1493–1499.
[3] M.Z. Zhang, Y. Wang, G.W. Yu, M. Wang, R.W. Peng, Y.Y. Weng, N.B. Ming, J. Phys. Condens. Matter 16 (2004) 695–704.
[4] R.J. Angels, D.B. Knorr, H.D. Merchant, J. Electron. Mater. 24 (1995) 927–933.
[5] S. Kang, J. Yang, D.N. Lee, Plat. Surf. Finish. 82 (1995) 67–70.
[6] D.N. Lee, S. Kang, J. Yang, Plat. Surf. Finish. 82 (1995) 76–79.
[7] J. Yang, D.N. Lee, Met. Mater. Int. 5 (1999) 465–470.
[8] U.F. Kocks, C.N. Tomé, H.R. Wenk (Eds.), Texture and anisotropy: preferred orientations in: Polycrystals and Their Effect on Materials Properties, Cambrige University Press, Cambrige, UK, 1998.
[9] J. Yang, S.Y. Kang, D.N. Lee, Met. Mater. Int. 3 (1997) 130–136.
[10] N. Murata, K. Tamakawa, K. Suzuki, H. Miura, in: Proceedings of the IMPACT Conference 2009 International 3D IC Conference, art. no. 5382211, pp. 436–439.
[11] N. Murata, K. Tamakawa, K. Suzuki, H. Miura, in: Proceedings of the 10th International Conference on Electronic Materials and Packaging, EMAP, 2008, art. no. 4784224, pp. 41–44.
[12] G. Khatibi, M. Klein, E. El-Magd, H.D. Merchant, B. Wesis, R. Wiechmann, P. Zimprich, IPC Expo 2001, Anaheim, CA, April 2001.
[13] H.D. Merchant, J. Electron. Mater. 24 (1995) 919–925.
[14] H.D. Merchant, J. Electron. Mater. 22 (1993) 631–638.
[15] H.D. Merchant, J. Electron. Mater. 33 (2004) 83–88.
[16] Y. Akiniwa, T. Suzuki, K. Tanaka, Mater. Sci. Forum 524–525 (2006) 807–812.
[17] V. Randle, G.L.F. Powell, J. Mater. Sci. 32 (1997) 561–565.
[18] W.C. Oliver, G.M. Pharr, J. Mater. Res. 7 (1992) 1564–1580.
[19] T.B. Massalski, H. Okamoto, P.R. Subramanian, L. Kacprzak, Binary Alloy Phase Diagrams, 2nd ed., ASM International, Materials Park, OH, 1990.
[20] J. Chastain, R.C. King Jr. (Eds.), Handbook of x-ray photoelectron spectroscopy, Physical Electronics, Inc., Eden Prairie, Minnesota, 1995.
[21] J.D. Verhoeven, Fundamentals of Physical Metallurgy, John Wiley and Sons, New York, 1975, Chap. 10, p. 325.
[22] T.H. Courtney, Mechanical Behavior of Materials, McGraw-HillCompanies, Inc., New York, 2000, p. 60 (Chapter 2).
[23] G.E. Dieter, Mechanical Metallurgy, SI Metric Ed., McGraw-Hill Companies, Inc., New York, 1988, p. 290 (Chapter 8).
[24] C. Mondal, A.K. Singh, A.K. Mukhopadhyay,and, K. Chattopadhyay, Mater. Sci. Forum 702–703 (2012) 303–306.

[25] L. Guo, Z. Chen, L. Gao, Mater. Sci. Eng. A 528 (2011) 8537–8545.
[26] J.D. Baird, in: R.E. Reed-Hill (Ed.), The Inhomogeneity of Plastic Deformation, ASM, Metals Park, OH, 1973, p. 191.
[27] A. Manonukul, F.P.E. Dunne, Acta Mater. 47 (2006) 4339–4354.
[28] L. Xiao, Scr. Metall. 22 (1988) 179–182.
[29] Y.C. Dong, I.V. Alexandrov, J.T. Wang, Mater. Sci. Forum 667–669 (2011) 891–896.
[30] G.E. Dieter, Mechanical Metallurgy, SI Metric Ed., McGraw-Hill Companies, Inc., New York, 1988, p. 202 (Chapter 6).